Cement and Concrete Research 93 (2017) 8–16

Contents lists available at ScienceDirect

Cement and Concrete Research

journal homepage: www.elsevier.com/locate/cemconres

Analysis of barium retention mechanisms on calcium silicate hydrate phases

Tiziana Missana *, Miguel García-Gutiérrez, Manuel Mingarro, Ursula Alonso

CIEMAT, Physical Chemistry of Actinides and Fission Products Unit, Department of Environment, Avenida Complutense 40, 28040 Madrid, Spain.

ARTICLE INFO

Article history:
Received 22 August 2016
Received in revised form 11 November 2016
Accepted 21 December 2016
Available online 7 January 2017

Keywords:
Calcium silicate hydrate (C-S-H) gels
Radioactive waste
Adsorption
Earth alkaline metals
Alkalis
Thermodynamic modelling

ABSTRACT

Calcium silicate hydrate (C-S-H) phases mostly contribute to contaminant retention in cement. The adsorption mechanisms of Ba on C-S-H phases with four different Ca/Si ratios were investigated by batch sorption experiments. The sorption kinetics, the effects of the solid to liquid ratio and the presence of alkalis in solution were analysed. Sorption isotherms in a wide range of Ba concentrations (from 10^{-10} to $1 \cdot 10^{-1}$ M) were performed. To understand the underlying retention mechanisms, the effects of Ba adsorption on surface potentials were additionally examined. The main objective of this study was to develop a sorption model able reproducing not only the Ba sorption behaviour, but also the C-S-H surface potential before and after Ba uptake. The reactions and model parameters selected for satisfying these conditions are discussed in the paper. A three-site model, with *weak* and *strong* silanol sites and one exchange site, which satisfactorily fulfils the initial aims, is proposed.

1. Introduction

Cement-based materials are widely used in radioactive waste repositories [1–5]. In fact, they have high sorption capacity for many contaminants, presenting different highly sorbing minerals; additionally, under the alkaline conditions generated by cement systems, many contaminants become much less soluble and mobile [6].

Calcium silicate hydrate (C-S-H) phases are the most relevant amongst the cement sorbing components: they represent between the 50 and 70% of the hardened cement paste (HCP), and due to their microstructure and high surface area (BET > 100 m^2/g), they control radionuclide retention in cements [7–9]. Other important hydration products of HCP are portlandite ($Ca(OH)_2$); Ettringite (AFt) or AFm phases [10].

The C-S-H phases (also called cement gels) are nano-sized materials usually amorphous or poorly crystalized and may have a variable chemical composition $xCaO \cdot SiO_2 \cdot yH_2O$, with $0.6 < x < 1.8$ approximately; the Ca/Si ratio is responsible of the different physical-chemical characteristics of the phases [11] during different stages of cement aging. The C-S-H structure is comparable to other more crystalline minerals like tobermorite or jennite, consisting on Ca-O central layers sandwiched by tetrahedral silicate layers [11–14]. The silicate chains are arranged following a pattern repeated every three tetrahedral (*dreierkette* structure): two of the three tetrahedra (paired) are linked together and share O-O edges with the central Ca-O; the third one (bridging) shares an oxygen atom at the pyramidal apex of Ca and connects paired tetrahedra. Increasing the Ca/Si ratio, the number of bridging tetrahedra decreases (being replaced by Ca ions), thus the C-S-H structure can be defined as a 'defect tobermorite structure' [15,13]. The region between layers (interlayer) hosts water molecules, calcium and other ions.

Ochs et al. [5] recently reviewed sorption data on cementitious material of several elements relevant for radioactive and industrial wastes, and provided a sorption coefficients database. Sorption values were linked to various stages of cement degradation, and possible underlying retention mechanisms were discussed. They considered strontium and radium as the most relevant divalent elements (M^{2+}) in the contest of radioactive waste disposals, and summarised the main studies existing on their sorption behaviour in cementitious materials [7,16–21]. The scarceness of data on radium retention was especially evidenced: indeed, for its long life (approximately 1600 years), ^{226}Ra is a critical radioisotope from an environmental point of view.

The mechanisms suggested by different authors for the retention of cations on cement, are different: from the complexation on deprotonated silanol groups [22], to its binding via cation exchange by stoichiometric replacement of Ca^{2+} by M^{2+} at the surface sites of C-S-H phases [19–20]. Wieland et al. [21] observed by XAFS studies in cement that Sr was sorbed mainly on C-S-H phases as partly hydrated species via two bridging oxygen atoms; however, they interpreted wet chemistry data using the classical ion exchange theory and neglecting specific uptake mechanisms.

It is generally agreed that sorption of earth alkaline ions in cementitious materials is strongly influenced by the aqueous Ca (the highest the

* Corresponding author.
E-mail addresses: tiziana.missana@ciemat.es (T. Missana), miguel.garcia@ciemat.es (M. García-Gutiérrez), m.mingarro@ciemat.es (M. Mingarro), ursula.alonso@ciemat.es (U. Alonso).

http://dx.doi.org/10.1016/j.cemconres.2016.12.004
0008-8846/

Ca content the lower sorption) and that other ions may also compete for sorbing sites. Alkalis, as sodium and potassium are of special importance, because their presence is often significant in cement porewater and furthermore they were observed to decrease M^{2+} sorption on C-S-H phases [15,19–20]. Other studies suggested different interactions of Cs (specific) or Na (indifferent) towards the C-S-H surface [23–24].

In this study, the sorption behaviour of Ba on C-S-H phases will be deeply analysed. Four phases with different Ca/Si ratio (from 0.8 to 1.6) will be used and characterized previous to retention tests. The main objective is to analyze the mechanisms of Ba sorption on these phases and to develop a sorption model being able simulating: a) Ba retention behaviour within the widest as possible range of tracer concentration; b) the possible competition effects on Ba sorption of alkali ions (Na, K and Cs) and c) to sketch the surface potential behaviour (trend and magnitude) of the materials before and after Ba adsorption. This last point is especially relevant to identify specific retention mechanisms.

To the best of our knowledge, previous studies on retention of Ba on C-S-H with modelling do not exist. The main advantage of using Ba, to improve the knowledge of retention mechanisms of alkaline earth elements in cementitious material (and especially Ra), are multiple. First of all, Ba and Ra have a very similar ion radius (1.34 Å and 1.43 Å) [25] and thus similar chemical behaviour. Barium can be used in a very wide range of concentrations, whereas the use of Ra must be limited to trace concentrations, for its very high radiotoxicity.

To extend the range of tracer concentration in sorption isotherms is fundamental to gather information on C-S-H phases sorption sites, which density is expected to be very large; furthermore the possible effects on the surface charge or potential, due to the incorporation of the element, can be detected only at relatively high sorbing element concentration ($>1 \cdot 10^{-3}$ M).

The whole experimental data will be interpreted by modelling and the advantages or limitation of possible different approaches will be discussed.

2. Materials and methods

2.1. C-S-H gels preparation and characterisation

Four C-S-H phases with different CaO/SiO_2 (Ca/Si) molar ratios were synthetized. The target Ca/Si ratios were: 0.8, 1, 1.2 and 1.6. The method used for producing the phases was the "*direct method*", as described in several papers [7,9,20].

The preparation was carried out in an anoxic glove box, under N_2 atmosphere ($O_2 < 1$ ppm). For their synthesis CaO (Alfa Aesar 99.95% purity) and SiO_2 (Aldrich 99.8% purity, surface area 175–225 m^2/g, as indicated by the supplier) were used. Both solids were weighted to obtain the requested molar Ca/Si ratios and a solid to liquid ratio of 10 or 20 g/L; afterwards they were mixed to 1 L deionised water previously boiled and bubbled with N_2 to minimize the CO_2 contamination.

The suspensions were prepared in HDPE dark bottles and maintained under stirring to obtain a homogeneous product [26]. Conductivity and pH were periodically measured until the steady-state was reached (10–15 days approximately), indicating the completion of the synthesis process.

Measurements of pH (± 0.10) were made using a Mettler Toledo (S220) pH-meter with a solid polymeric electrode (Xerolyt) or a Crison pH-ion meter (GLP225) with a combined glass pH electrode (Metrohm). Electrodes calibration was made with buffer solutions at pH 2.00, 4.00, 7.00, and 10.00. Conductivity measurements were carried out with a Crison EC Meter Basic 30^+.

The final pH and conductivity of gel suspensions are specific for each Ca/Si ratio and summarised in Table 1. Sorption experiments and ζ-potential measurements were carried out directly with these suspensions.

Upon the formation of the C-S-H phases, an aliquot of 250 mL of each suspension was filtered by 0.1 μm. Part of the supernatant (50 mL) was used for Ca and Si quantification, and the other fraction stored for its use for dilutions. Ca and Si in the supernatant were measured by ICP-OES with a VARIAN 735ES spectrometer. The filtered solid was used for further analyses. In some cases, the solid was previously "washed" with ethanol and deionised water before the measurement.

The C-S-H surface area was measured by N_2-BET, their composition and homogeneity by (micro)proton induced X-ray emission (μPIXE). μPIXE measurements were carried out at the nuclear microprobe facility at the Laboratori Nazionali di Legnaro (INFN-LNL) in sample area of 2×2 mm^2.

Atomic force microscopy (AFM), in tapping mode, was used to analyze their microstructure with a Nanoscope IIIa apparatus (Digital Instruments). AFM samples were prepared depositing a drop of the suspensions onto a freshly cleaved mica substrate (after Poly-L-Lysine coating) and left drying in the anoxic chamber under N_2 atmosphere overnight. AFM image analysis was carried out with the WSXM 4.0 software [27].

2.2. C-S-H gels surface charge measurement

The ζ-potential of the C-S-H phases (initial and upon Ba addition) was measured by means of the laser Doppler electrophoresis technique using a Malvern Zetamaster apparatus equipped with a 5-mW He-Ne laser ($\lambda = 633$ nm, scattering angle 90°). The samples in which radioactive tracer was adsorbed, were analysed with a ZetaSizer Nano ZS (Malvern) (He-Ne laser, $\lambda = 633$ nm, scattering angle 173°) available in the radioactive laboratory. This apparatus allows the measurement of both particle size and ζ-potential. In all the C-S-H phases, the suspended particles were observed to form large aggregates with size >1 μm. In fact, the water in equilibrium with the gels has relatively high salinity and calcium content, these factors favouring particle aggregation.

To measure the variation of the surface potential upon Ba addition, the C-S-H phases were contacted with the tracer during three days and maintained under stirring. Measurements of ζ-potential were carried out using the original suspensions at 10 g/L, to mimic the conditions of sorption isotherms, or diluted to 1 g/L, to facilitate ζ-potential measurements. The aggregated particles sediment very fast, making the measurement difficult.

The ζ-potential was calculated from the measured electrophoretic mobility using the Smoluchowski equation [28].

Table 1
Chemical analyses of the solid or supernatant of the C-S-H phases.

Sample	pH	Conductivity (μS/cm)	Ca (mg/L)	Si ppm (mg/L)	Ca/Si (μPIXE)	N_2-BET (m^2/g)
C-S-H (0.8) 10 g/L	10.38	201	44	75	0.89 ± 0.04	200 ± 3
C-S-H (0.8) 20 g/L	10.36	202	45	84	n.d.	n.d.
C-S-H (1.0) 10 g/L	11.41	926	82	4	1.03 ± 0.04	124 ± 2
C-S-H (1.2) 10 g/L	12.19	2140	204	1.5	1.26 ± 0.15	109 ± 2
C-S-H (1.6) 10 g/L	12.37	6240	600	0.2	1.60 ± 0.11[a]	73 ± 1

[a] After washing.

2.3. Radionuclide and counting techniques

The radionuclide used was ^{133}Ba, supplied by Eckert and Ziegler Isotope Products. Ba comes as $BaCl_2$ in HCl 0.1 M with a carrier of stable Ba (10 μg/mL solution). ^{133}Ba has half-life of 10.51 years; it decays by electron capture and presents different gamma emissions from 0.03 and 0.4 MeV. Its activity in solution was measured by γ-counting with a NaI detector (Packard Autogamma COBRA II). The uncertainty for the counting procedure is <2%. The detection limit is approximately $5 \cdot 10^{-12}$ M.

2.4. Sorption tests

Sorption data were obtained using a batch sorption technique. Experiments with the C-S-H phases were carried out in anoxic glove box under N_2 atmosphere and at room temperature. The C-S-H suspensions were used *as prepared* (10 g/L or 20 g/L) or diluted with their own contact water, previously separated by filtering. The sorption dependence on solid to liquid (S/L) ratio, radionuclide concentration and the presence of alkalis in solution was analysed, as well as the kinetics of the sorption process.

The kinetics of the sorption process was investigated first, on the C-S-H phases with Ca/Si 0.8 and 1, at 10 g/L, to determine the time required for the attainment of sorption equilibrium. The suspensions (10 mL), were introduced in centrifuge tubes, traced with ^{233}Ba and maintained in continuous stirring during the selected contact time (from 1 h to 30 days). The effect of S/L was analysed with suspensions of C-S-H (0.8) from 0.45 to 20 g/L and a contact time of 10 days.

The effect of the presence of alkali ions (M^+ = Na, K and Cs) on Ba adsorption was analysed measuring the Ba distribution coefficient upon the addition of different quantities (from approximately $1 \cdot 10^{-3}$ to $5 \cdot 10^{-2}$ M) of NaCl, KCl or CsCl to the C-S-H (0.8) previously phase traced with Ba. In these tests, the tracer concentration was [Ba] = $3.4 \cdot 10^{-10}$ M.

After the desired contact time, the solid and liquid phases were separated by centrifuging (25,000*g*, 30 min), with a JOUAN MR23i centrifuge. After the solid separation, three aliquots of the supernatant were extracted from each tube for the analysis of the final Ba activity. The rest of the solution was used to check the final pH.

Sorption isotherms were carried out by varying the radionuclide concentration from [Ba] = $1 \cdot 10^{-10}$ M to [Ba] = $1 \cdot 10^{-3}$ M, approximately, with a S/L of 10 g/L. The highest concentrations were achieved adding stable Ba in the form of $BaCl_2$. A sorption isotherm with C-S-H (1) was carried out in a wider range of Ba concentration (up to approximately 0.1 M), to improve the modelling of data at high sorbate concentration and to cross-check the information on surface potential with sorption data. The measurements of the ζ-potential, after Ba addition, were carried out with Ba concentration from $1 \cdot 10^{-3}$ to $5 \cdot 10^{-2}$ M approximately.

Solid/supernatant separation procedure was the same as previously described. The degree of sorption was quantified by the distribution coefficient K_d ($mL \cdot g^{-1}$), defined as the ratio of the mass (activity) of the element per unit mass of the solid to the mass (activity) per unit volume of the solution. It is calculated with this formula:

$$K_d = \frac{C_{in} - C_{fin}}{C_{fin}} \cdot \frac{V}{m} \quad (1)$$

C_{in} and C_{fin} are the initial and final concentrations of Ba in the liquid phase ($Bq \cdot mL^{-1}$), m the mass of the gel (g) and V the volume of the liquid (mL).

Sorption onto vials and ultracentrifuge tubes was checked after sorption experiments. Sorption of Ba onto these vessels was always lower than 2% and therefore it was not accounted for in K_d calculations.

2.5. Modelling

The objective of the modelling exercise is to reproduce all the experimental sorption data and to sketch the main charge behaviour of C-S-H phases experimentally observed before and after Ba adsorption.

The existence of silanol groups (SiOH) on the C-S-H surface is usually assumed [9,29–31] and the sorption of inorganic species on silanol surface groups can be described in terms of surface complexation reactions.

The classical diffuse double layer model (DLM) [32–33], is generally applied to describe the surface of oxides and their complexation with ionic species, and it can be also used with other materials, including C-S-H gels.

In the diffuse DLM, the surface charge density (σ, C/m^2), is determined by all the surface coordination reaction with cations and/or anions and the distribution of ions in the diffuse layer follows the Gouy-Chapman equation. The relation between the surface charge and the surface potential (Ψ) is given by the following relation:

$$\sigma = \left(8RT\varepsilon\varepsilon_0 c \cdot 10^3\right)^{1/2} \sinh(Z\Psi F/2RT) \quad (2)$$

R is the molar gas constant, T the absolute temperature, ε the dielectric constant of water, Z the valence of the electrolyte, F the Faraday constant, ε_0 the vacuum permittivity and c the molar electrolyte concentration. The values of potentials, were calculated from this relation using the geochemical CHESS v 2.4 code [34–35].

Under alkaline conditions, silanol groups are deprotonated according to this reaction:

$$SiOH \underset{K1}{\Leftrightarrow} SiO^- + H^+ \quad (3)$$

The intrinsic equilibrium constant of this reaction is K_1, being the mass law equation corresponding to the reaction (3):

$$K_1 = \frac{(SiO^-)\{H^+\}}{(SiOH)} \exp\left(-\frac{F\psi}{RT}\right) \quad (4)$$

where {} represent the ion the activity and () ion concentration. The activity coefficients for the surface species are assumed to be 1. The exponential represents the coulombic term accounting for the electrostatic effects [33].

The experimental determination of the potential (Ψ) is not straightforward. Nevertheless, an estimation of this potential can be done through the experimental measurement of the electrokinetic or zeta (ζ)-potential. Even ζ-potential values (which refer to the potential at the *shear-plane*), do not provide direct measurement of Ψ (which refers to the *diffuse layer plane*, or distance of closest approach for background electrolyte ions), they approximate well when potentials are low [28]. Furthermore ζ-potential is very useful to obtain information on the sign of the surface charge and/or points of zero charge (PZC), under different conditions.

In the literature dealing with the description of the surface of C-S-H phases, there is not a common agreement on the acid-base properties of silanol groups and a large variability on reported K_1 (Eq. (4)) exists. For example, Heat et al. [36] considered a pK_1 value of 6.8; Viallis and Terrise [23] of 12.3; Pointeau et al. [9,29] of 12. Labbez et al. [30] used the value of the first dissociation constant of the silicic acid (9.8). Churacov et al. [37] obtained the surface acidity constants of silanol groups in C-S-H by ab-initio calculations. They considered four different possible structural positions for these groups in C-S-H and obtained four different pK_1 varying from 5.52 to 11.87. Therefore, a common agreement on the properties of silanols in C-S-H does not exist.

In this work, the pK_1 value reported in the literature for the silanol groups of the amorphous silica (6.8 ± 0.5) [38–39] will be used. Amorphous silica is indeed the main precursor of C-S-H phases. The parameters that will be used for the modelling are summarised in Table 2.

Table 2
Reactions and parameters used for sorption modelling.

Description	Reaction	LogK (value and reference)		Density (value and reference)	
Silanol (weak site)	$SiOH \Leftrightarrow SiO^- + H^+$	6.80 ± 0.5	Papirer (2000)	13 μmol/m^2	This work
Silanol (strong site)	$Si_sOH \Leftrightarrow Si_sO^- + H^+$	6.80 ± 0.5	Papirer (2000)	0.0035 μmol/m^2	This work
Exchange site	X_2Ca			2 μmol/m^2	This work
Complexation of Ca (CSH charge)	$SiO^- + Ca^{2+} \Leftrightarrow SiOCa^+$	−4.12	Calculated This work		

Description	Reaction	LogK	Reference
Ba adsorption			
Complexation of Ba on weak sites	$SiO^- + Ba^{2+} \Leftrightarrow SiOBa^+$	−4.5	This work
Complexation of Ba on strong sites	$Si_sO^- + Ba^{2+} \Leftrightarrow Si_sOBa^+$	−0.3	This work
Ba exchange	$X_2Ca + Ba^{2+} \Leftrightarrow X_2Ba + Ca^{2+}$	1.3	This work

Description	Reaction	LogK			Reference
		Na	Cs	K	
Alkali adsorption on C-S-H (0.8)					
Complexation of M^+ on weak sites	$SiO^- + M^+ \Leftrightarrow SiOM$	−5.50	−5.40	−5.40	This work
Complexation of M^+ on strong sites	$Si_sO^- + M^+ \Leftrightarrow Si_sOM$	−5.00	−1.75	−1.60	This work
M^+ exchange	$X_2Ca + 2\,M^+ \Leftrightarrow 2XM + Ca^{2+}$	0.37	0.27	0.37	This work

In the DLM approximation, the complexation of the ion M^{z+} with silanol sites is expressed by the reaction:

$$SiOH + M^{z+} \underset{K_{C,M}}{\Leftrightarrow} SiOM^{z-1} + H^+ \quad (5)$$

with the intrinsic equilibrium $K_{C,M}$ (complexation constant of M):

$$K_{C,M} = \frac{\left(SiOM^{z-1}\right)\{H^+\}}{(SiOH)\{M^{z+}\}} \exp\left(-\frac{F\psi}{RT}\right) \quad (6)$$

As already mentioned in the introduction, many authors consider the possibility that (divalent) cations can also replace Ca^{2+} in C-S-H phases structure (or that of their homologues like tobermorite [40–41]), conferring to these materials ion-exchange properties.

In previous works [7,20] the retention of divalent strontium and radium on C-S-H phases was described considering a single site cation exchange model where M^{2+} exchange with Ca^{2+} present at the C-S-H surface according to this reaction [7]:

$$X_2Ca + M^{2+} \leftrightarrow X_2M + Ca^{2+} \quad (7)$$

The selectivity coefficient for this reaction is defined by:

$${}_{Ca}K_C = \frac{N_{M^{2+}}}{N_{Ca}} \frac{\left[Ca^{2+}\right]}{\left[M^{2+}\right]} \quad (8)$$

where N_M^{2+} represents the equivalent fractional occupancy of the ion M^{2+}, which can be expressed by $N_{M^{2+}} = \frac{2*\{M^{2+}\}}{CEC}$, where $\{M^{2+}\}$ is the amount of divalent cation adsorbed (mol/Kg) and CEC is the cation exchange capacity of the material (eq/Kg). The relation between the K_d of Ba (if sorption is attributed to cationic exchange) and the Ba-Ca selectivity coefficient is given by:

$$K_d = \frac{0.5 * CEC^{*Ba}_{Ca} Kc}{\left[Ca^{2+}\right]}$$

The density of surface sites (or CEC for ionic exchange) is another very important parameter for the modelling. For amorphous silica or silica gels the reported surface density ranges from 4.5 to 25 sites/nm^2 [42–43]. For C-S-H, values reported in the literature range between approximately 5 and 10 sites/nm^2 [7,9,30].

These gels possess a very high density of surface sites, but experimental studies for determining this parameter are scarce and some discordance of literature data is also found. An attempt to better estimate the density of sorption sites in our C-S-H phases was done, by the analyses of the sorption isotherm with high Ba concentration trying to evidence the saturation of sorption sites.

Different models will be tested trying to reproduce the adsorption behaviour in the different C-S-H phases and their surface charge upon adsorption. Modelling calculations were aided by CHESS v 2.4 code [34].

3. Results and discussion

3.1. Solid characterisation

The BET area of the samples was measured by N_2 adsorption: the mean N_2-BET value measured for C-S-H phases with Ca/Si 0.8, 1 and 1.2 was 144 ± 40 m^2/g, very similar to that proposed by Tits et al. [7], 148 m^2/g, but the value measured in the C-H-S (1.6) was approximately halved (73 m^2/g). This was the first indication that some process, that may affect sorption, is occurring as the Ca/Si increases beyond a certain value. Surface area measurements were repeated after washing the solids with water-ethanol. The mean N_2-BET value for the first three phases did not change significantly, but the surface area of the washed C-S-H (1.6) increased up to 144 m^2/g. This means that some other soluble mineral with much lower surface area may be present in this gel suspension.

μPIXE measurements of the Ca/Si ratio of C-S-H phases with Ca/Si ratio of 0.8, 1 and 1.2 were very well in agreement with the target values (Table 1) and, in these samples, Ca and Si were distributed fairly homogeneously. On the other hand, the element distribution maps of the C-S-H (1.6) showed regions of clear Ca excess (Ca/Si > 2), possibly indicating the precipitation of a Ca-bearing mineral, most probably portlandite, formed during the synthesis of the gel [23]. Other studies [12,15] reported the difficulty of synthetizing C-S-H phases with Ca/Si > 1.5 without portlandite (co)precipitation and this obviously may affect the overall sorption properties of the material.

μPIXE measurements of the C-S-H (1.6) were also repeated with the washed sample. In this case, Ca and Si were more uniformly distributed and their ratio was in agreement with the theoretically expected (Table 1).

The morphology of the gel particles was analysed by AFM. Fig. 1 shows the AFM images of the SiO_2 used for the gels preparation (Fig. 1a) and of the C-S-H phases with Ca/Si of 0.8; 1.2 and 1.6 (Fig. 1b, c and d, respectively). The mean particle size of the SiO_2 is lower than 50 nm.

The microstructure of the C-S-H gels, as observed by AFM, is similar for phases with Ca/Si < 1.2. Large aggregated of particles in the nanometre range (50–200) sometimes with a *piled-up* structure are always observed. For the C-S-H (1.6) phase (Fig. 1d) different structures, more ordered (and somewhat denser) are also superimposed. AFM analysis of C-S-H (1.6) seem also indicating the presence of larger crystals, covered by smaller particles. These observations are in agreement with the measured decrease of the BET area for the C-S-H (1.6) phase and also with the possible precipitation of Ca-bearing minerals.

3.2. Sorption tests

The results of sorption tests as a function of time and solid to liquid ratio are shown in Fig. 2. The sorption equilibrium is reached approximately in 3 days (Fig. 2a), which was considered the minimum contact time needed for further sorption experiments. A slight sorption increase is observed as the solid to liquid ratio increases (Fig. 2b), but the variation is within the experimental error, thus the effect of this parameter within the range of gel concentration from 0.45 to 20 g/L is negligible. The solid to liquid ratio selected for further experiments was 10 g/L.

Fig. 3 shows Ba sorption isotherms, on the four C-S-H phases, obtained varying Ba concentration from approximately $1 \cdot 10^{-10}$ to $1 \cdot 10^{-3}$ M. Data are expressed both as logarithm of the distribution coefficient vs. logarithm of aqueous Ba at the equilibrium (Ba_{eq}, M), in Fig. 3a, and as logarithm of the adsorbed Ba (Ba_{ads}, Mol/g) vs. logarithm of Ba_{eq}, in Fig. 3b.

First of all, sorption is linear up to initial Ba concentrations of approximately 10^{-6} M ($[Ba_{eq}] \sim 10^{-8}$ M), then a decrease in distribution coefficients is observed. Furthermore, sorption decreases when the Ca/Si ratio of the gels increases, i.e. with the increase of the aqueous Ca in solution (Table 1). This result is in agreement with data previously reported by other authors for divalent cations [7,20,22] and points out the important role that Ca plays on alkali metals retention in these materials.

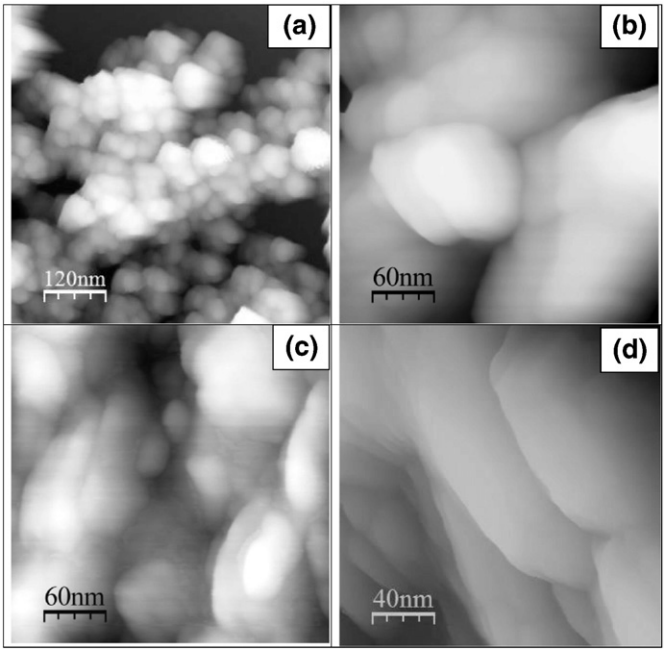

Fig. 1. AFM pictures of: (a) SiO_2 used for the gels preparation; (b) C-S-H (0.8); (c) C-S-H (1.2) and (d) C-S-H (1.6).

The dependence of the $LogK_d$ (from the mean values of the linear zone at low Ba loadings, from Fig. 3a) on the logarithm of the aqueous Ca concentration is shown in Fig. 4. This dependence is linear (with the slope of −0.9) for the C-S-H phases with Ca/Si of 0.8, 1 and 1.2. In principle, this observed dependence could be related to Ca-Ba cationic exchange process (2:2) and indicates that sorption mechanism affecting Ba retention are similar in these phases. In contrast, the behaviour of the C-S-H (1.6) deviates from that of the other phases showing less sorption capacity. This can be in agreement with the presence of portlandite in the suspension, as suggested by the previous result (BET and μPIXE), which is a less sorbing mineral than C-S-H.

Tits et al. [20] also observed that the calculated Sr-Ca selectivity coefficient in the C-S-H (1.6) was significantly smaller than the one of phases with lower Ca/Si and they concluded that formation of portlandite may have occurred, causing artefacts in sorption measurements.

3.3. Modelling and interpretation of sorption and ζ-potential data

The sorption model to be developed must take into account the sorption behaviour in the all range of Ba concentration (including the dependence on aqueous Ca) and be able reproducing, at least *grosso modo*, the charge behaviour of the untreated C-S-H phases and after Ba adsorption. Fig. 5 shows the ζ-potential measured on the four C-S-H phases without any treatment (Fig. 5a) and after the addition of Ba (Fig. 5b).

The ζ-potential of the untreated phases is plotted as a function of the aqueous Ca; as already mentioned, the increase in the Ca/Si ratio leads to an increase of the aqueous Ca in the supernatant (Table 1). The ζ-potential increases as the Ca/Si ratio (or aqueous Ca) increases, and the sign of the potential changes from negative to positive at a concentration of Ca of approximately 110–130 ppm (approx. 3 mM). The magnitude of the measured ζ-potential is not very large (between −15 and 15 mV approximately), but its variation is clear.

This behaviour has been already observed by other authors [23,44] and it can be interpreted considering that Ca is a potential determining ion of the C-S-H phases and that the surface charge arises by the balance of silanol deprotonation (Eq. (3), SiO^-) and Ca complexation onto the silanols (Eq. (5), $SiOCa^+$). Other authors [30,45] rejected the hypothesis of specific adsorption of Ca on the C-S-H phases and consider that the charge is due to physical (electrostatic) interactions and not to chemical adsorption.

However, if the charge of the C-S-H phases is produced by the adsorption of the ion Ca (as potential determining ion) the point in which the charge (or surface potential) is zero is determined by the condition $(SiO^-) = (SiOCa^+)$, i.e. when the concentration of surface species negatively charged is equal to the concentration of positively charged species. Considering Eqs. (4) and (6) this condition is verified when $K_1/K_{C,Ca}$ is equal to the activity of Ca^{2+} at the PCZ ($2.1 \cdot 10^{-3}$ M). Therefore, if $logK_1 = 6.8$ (Table 2), $LogK_{C,Ca}$ must be −4.12.

The measured ζ-potentials were compared to the diffuse potential calculated by DLM (Eq. (2)) (valid approximation as ($|\zeta| < 15$ mV). The diffuse potential calculated using the abovementioned constants for $logK_1$ and $LogK_{C,Ca}$ (Table 2), and fixing the experimental pH and Ca concentrations (Table 1) is represented in Fig. 2 as a star, for each C-S-H phase. As can be seen in Fig. 2, the calculated potentials agree quite well with the measured ζ-potential, and also with the hypothesis that the surface charge arises by the specific adsorption of the ion Ca^{2+}.

Fig. 5b shows the ζ-potential of the four C-S-H phases upon the addition of increasing quantities of Ba. It can be seen that the interaction of Ba with the C-S-H phases causes a progressive increase of the ζ-potential: from −15 to 0.5 mV in C-S-H (0.8); from −5 to 13 mV in C-S-H (1); from 5 to 18 mV in C-S-H (1.2) and from 11 to 22 mV in C-S-H (1.6). Thus, Ba retention in C-S-H gels causes an increment of the overall positive charge of the system; this result will be accounted for in the model and will help clarifying which type of mechanism might be

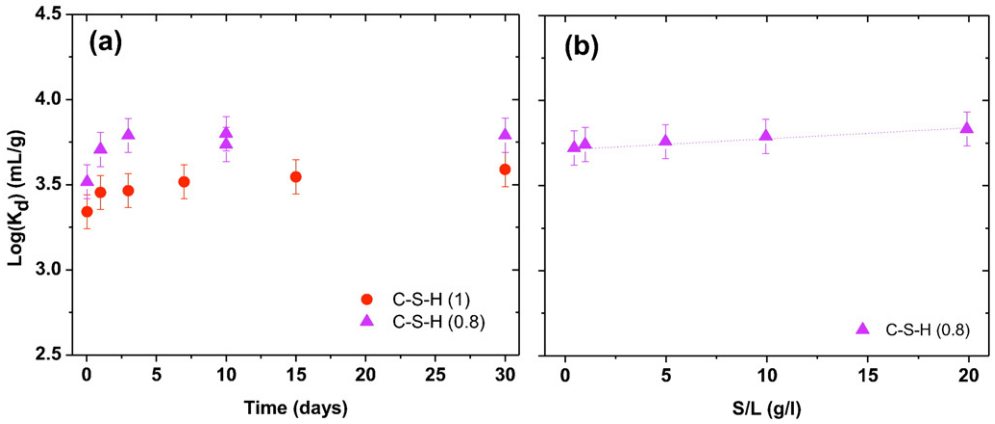

Fig. 2. (a) Ba sorption kinetics on (▲) C-S-H (0.8) and (●) C-S-H (1) at 10 g/L and (b) Sorption dependence on the solid to liquid ratio with (▲) C-S-H (0.8). [Ba] = $3.4 \cdot 10^{-10}$ M.

involved in Ba retention. Again, even after Ba adsorption, absolute values of the ζ-potentials are not very high, with a maximum measured value of about 20 mV.

To support the development of the sorption model, a sorption isotherm reaching very high Ba concentration (0.1 M) was carried out with C-S-H (1). This will also help interpreting the data of ζ-potential upon Ba adsorption (Fig. 5a).

This *full* sorption isotherm is plotted in Fig. 6a. Different possible sorption models were tested on these data and evaluated taking into account also the corresponding calculated surface potential (which was compared to the experimental ζ-potential).

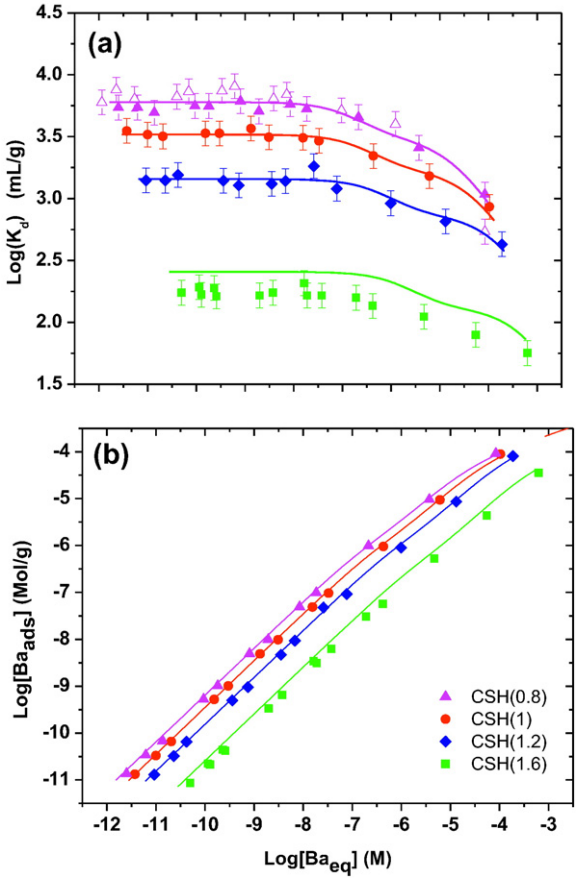

Fig. 3. (a) Ba sorption isotherms on (▲) C-S-H (0.8); (●) C-S-H (1); (◆) C-S-H (1.2) and (■) C-S-H (1.6) at 10 g/L; (△) C-S-H (0.8) at 20 g/L. Contact time 10 days. The continuous lines correspond to data fit with the parameters of Table 2.

Tits et al. [7,19,20] modelled the sorption data of Sr and Ra on C-S-H phases considering cationic exchange with Ca, and using a single site exchange model. Their C-S-H phases had a BET area of 148 m^2/g and they considered 5 sites/nm^2 as site density (approx. 8.0 μmol/m^2). The logarithm of the selectivity coefficient they obtained for Sr and Ra was 0.08 and 0.78, respectively.

Considering this approximation (Eq. (7)), with the same BET and site density proposed by Tits, the best fit of our experimental data, was obtained with a logarithm of the selectivity coefficient of 1.05 (similar to that reported by Tits (2006) for Ra), the best fit is plotted in Fig. 5a with magenta stars.

It can be seen that this *one site exchange* model, reproduces fairly well the experimental sorption data at the lowest and highest Ba concentrations, but clearly over-predicts our sorption data in the intermediate range of Ba concentration. The comparison between model and experimental data therefore suggests that more than one sorption site probably exists and that the density of sites used is slightly lower than the real one (as the slope of experimental data at the highest Ba loadings is lower than the simulated one).

Besides, the adsorption of Ba exclusively by ionic exchange will not produce any change of the charge (or potential) of the C-S-H surface, as shown in Fig. 6b. Thus, this last result is not in agreement with the experimental ζ-potential data of Fig. 5b, where a clear increment of the positive charge was observed upon Ba adsorption (and even charge inversion at the highest Ba loadings, in some C-S-H phases), so that other mechanism(s) must be accounted for.

To explain Ba retention on the C-S-H phases, surface complexation on silanol sites will be then considered. As alkaline earth ion, it is not

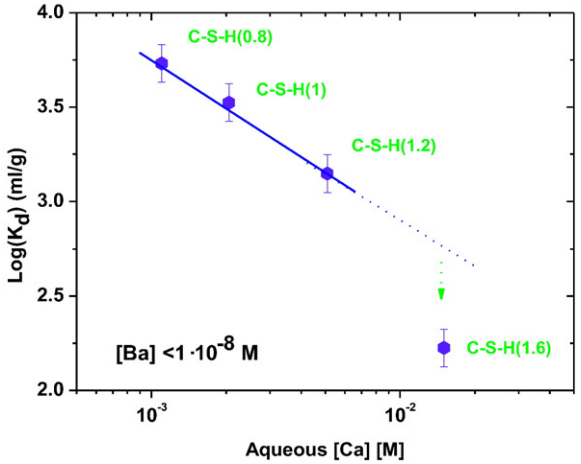

Fig. 4. Dependence of Ba distribution coefficients on the aqueous Ca content in the different C-S-H phases.

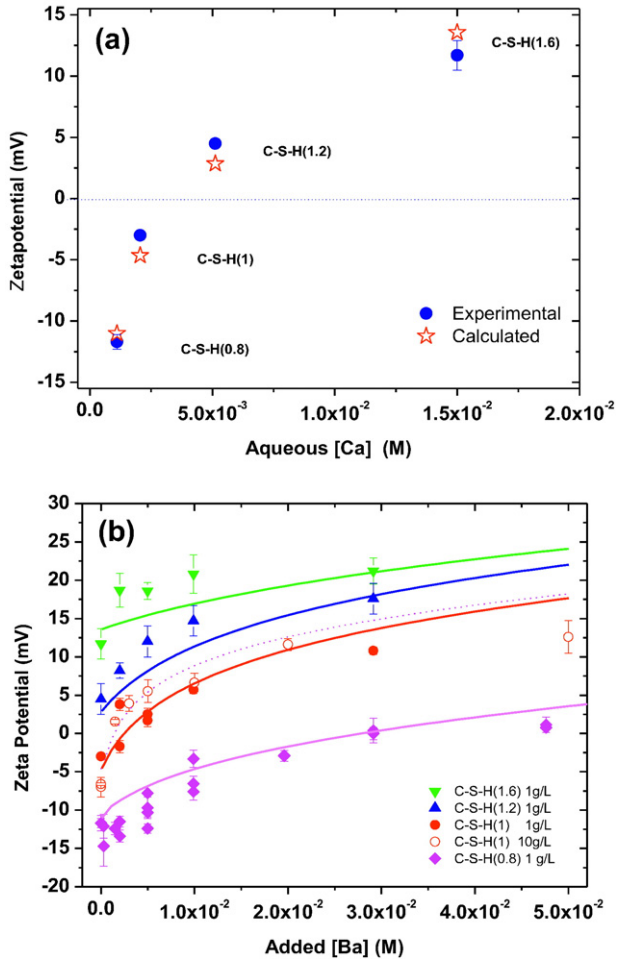

Fig. 5. (a) ζ-potential measured on the untreated C-S-H suspensions (10 g/L) as a function of their aqueous Ca content. The stars correspond to the surface potential calculated by the DLM with the data of Table 2. (b) ζ-potential measured on the different C-S-H phases as a function of the Ba content (after 3 days Ba/C-S-H contact time). The lines correspond to the potential calculated with the DLM.

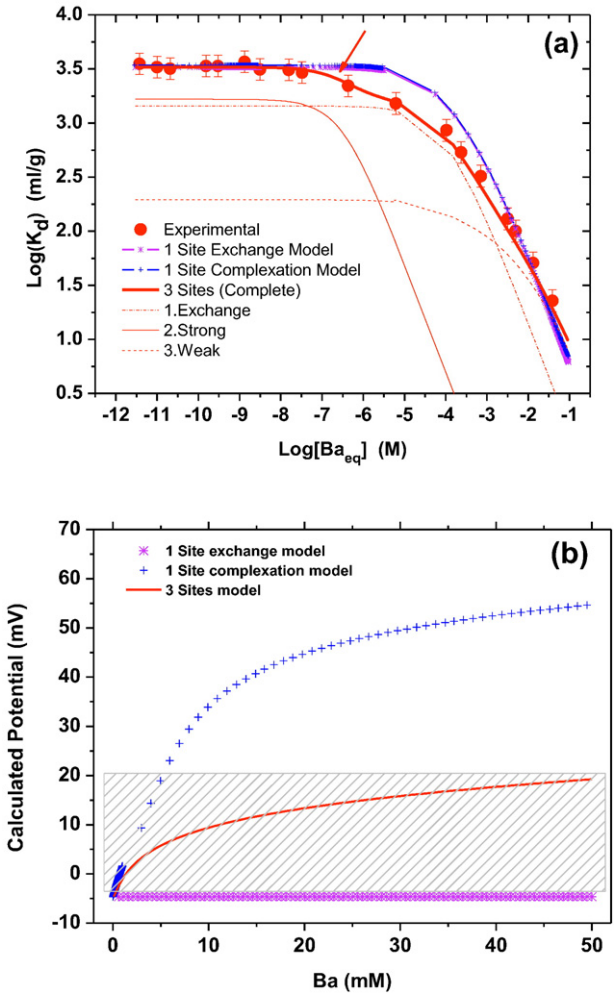

Fig. 6. (a) Sorption isotherms of Ba on C-S-H (1) and tentative modelling approaches of sorption data. (b) Surface potential as a function of the Ba content calculated considering the different modelling approaches. The grey box indicates the range of experimental ζ-potential values.

unlikely that Ba behaves similarly as Ca, thus it adsorption on the CSH phases should be expressed (at least partly) by the reaction:

$$SiOH + Ba^{2+} \underset{K_{C,Ba}}{\Longleftrightarrow} SiOM^{+} + H^{+} \quad (5b)$$

Considering Eq. (5b) (only one sorption site) and the same site density as that used in the first modelling attempt (5 sites/nm^2), the best fit of the data was obtained with the value of log$K_{C,Ba}$ of −3.05. This simulation is plotted in Fig. 6a as blue crosses. This simulation is completely equivalent (it is, in fact, superimposed) to the previous one and thus, also in this case, it is clear that one site is not enough to perfectly reproduce the experimental data, especially in the intermediate range of Ba concentrations, and that the surface density is slightly higher than that adopted for the modelling.

At the highest Ba concentrations, the simulation may be improved fixing the surface density for the silanols to a value of approximately 7.83 sites/nm^2 (13 μmol/m^2), which is in the range of those reported in the literature, as previously discussed.

Indeed, the complexation of Ba with silanols (Eq. (5b)) would lead to an increment of the surface potential (see the calculation in Fig. 6b), as observed experimentally. However, the magnitude of the calculated potential, at the highest Ba loadings, is significantly higher (60 mV) than the measured ζ-potential (around 15 mV), thus some additional variations in the model are needed.

To improve the agreement between the experimental ζ-potential data and the calculated ones, the log$K_{C,Ba}$ must be decreased. Reiterative calculations to fit both the surface potential and sorption data at the highest Ba loadings were performed to fix the log$K_{C,Ba}$ of reaction (5b).

A reasonable good fit of the experimental ζ-potential data could be obtained with values of log$K_{C,Ba}$ between −4 and −5. For C-S-H (0.8) log$K_{C,Ba}$ = −5; for C-S-H (1) log$K_{C,Ba}$ = −4.45 and for C-S-H (1.2) and C-S-H (1.6) log$K_{C,Ba}$ = −4.3. The continuous lines in Fig. 5b represent the calculated surface potential, using these values.

The mean value of log$K_{C,Ba}$ = −4.5 was fixed for further simulation of sorption data. It is interesting noticing that this value is only slightly lower than that determined for Ca (−4.12), suggesting similar behaviour of both alkaline earth elements.

In order to adequately fit the experimental data of the isotherm (Fig. 6a) and to find an agreement with ζ-potential data of Fig. 5b, two additional sorption sites were needed. The selected option was to include a strong silanol site (S_sOH) to reproduce the first bending of the isotherm (marked with an arrow in Fig. 6a). The selection of the complexation mechanism for Ba on this site might be arbitrary as the overall charge of the system is not varied, due to the low site concentration (0.0035 μmol/m^2). Additionally, the addition of a third sorption site with a density of 2 μmol/m^2, was required to fit completely the data.

From a pure modelling point of view, the selection of ionic exchange or surface complexation, as a sorption mechanism for the third sorption

site, results in equivalently acceptable fits of adsorption data, but not of ζ-potential data. The whole of data was better fit assuming that sorption on the third site occurs by ionic exchange.

The coexistence of both surface complexation and ionic exchange is not surprising, taking into account the structure of these phases, which present some analogies with clays (layered structure, presence of silanols).

The cation exchange with the ion Ca, hypothesized by the present model, can take place within the interlayer or in the external surface of the C-S-H particles. On the other hand, different environments for silica were reported in the literature (up to four in ^{29}Si NMR spectroscopy [46]), depending on their position in the silicate chain: for example in paired or bridging tetrahedra, at end of chains or in structural defects. Consequently different environments for silanols can be also assumed [15,37,46].

Yet, only two different silanol-like sites where enough to simulate Ba sorption data. Thus, it seems that independently of their position in C-S-H microstructure, most of them show similar sorption selectivity for Ba; only a very small portion (<0.3‰) presents much higher selectivity. Because of their very low density, it is very difficult to determine experimentally the location of these highly selective sorption sites.

The complete three-site model is plotted in Fig. 6a, as a continuous line, and the contribution to sorption of each site is also indicated. As mentioned, for the "weak" silanol sites $\log K_{C,Ba} = -4.5$; for the "strong" silanol sites $\log K_{C,Ba(strong)} = -0.3$; and for the exchange mechanism a selectivity coefficient of 1.3.

The calculated potential for C-S-H (1) obtained with this model as a function of Ba concentration is shown in Fig. 6b and compared with other modelling approaches; it agrees well (both in magnitude and trend) with the experimental ζ-potential data. Furthermore, Fig. 5b shows that this approach is valid also for all the other C-S-H phases.

The selected parameters for the final Ba sorption model are summarised in Table 2. With this model, all the isotherms presented in Fig. 3(a, b) were also simulated, and the continuous lines correspond to the fit for each phase. As can be seen, the model is able to reproduce very well the sorption data for the phases with Ca/Si ratio 0.8, 1 and 1.2 and slightly over-predicts sorption for the C-S-H (1.6). This phase, which presents significantly less surface area than the others, behaves as it had 65% less sorption sites (this value being calculated normalizing sorption values to the mean N_2-BET area of the other phases).

3.4. Ba sorption in the presence of alkalis

Finally, the effect of the presence of alkali ions (M^+ = Na, K and Cs) on Ba adsorption was analysed by measuring the Ba distribution coefficients upon the addition of different quantity of NaCl, KCl or CsCl. The experimental results are shown in Fig. 7.

Results show that at low alkali concentration, the competition effects are scarce as the decrease in distribution coefficient is limited (even not negligible). However, the presence of M^+ in solution at relatively high concentrations clearly decreases the sorption of Ba. At a concentration of approximately $[M^+] = 5 \cdot 10^{-2}$ M the logK_d of Ba, which is 3.8 in the absence of alkali, decreased to 3, 2.9 and 2.7 in the presence of Na, Cs and K respectively. Thus, the most competitive ion for Ba adsorption in C-S-H is K, followed by Cs and Na.

In previous studies [15,23–24] it was reported that Cs and Na may have different interactions with the C-S-H surfaces: the first interacting specifically, the second behaving as an indifferent electrolyte. However, considering the shape of Ba adsorption curves, the effect produced by the different alkalis on Ba adsorption seem to be similar (or produced by similar retention mechanisms); the main difference consists on the magnitude of the competition effect, related to the different affinity of the metals with the C-S-H surface.

To explain Ba sorption behaviour as a function of the M^+ concentration, as observed in Fig. 7, a three sites model (similar to that proposed in this study for Ba) was adopted, thus considering both surface complexation and ionic exchange as mechanisms responsible for alkali retention in C-S-H gels.

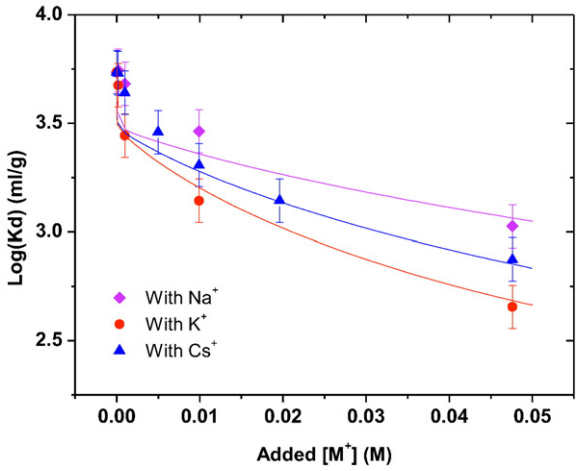

Fig. 7. Effect of the presence of the alkalis (◆) Na, (▲) Cs and (●) K on the distribution coefficient of Ba in C-S-H (0.8). Continuous lines correspond to the simulation of the curve with the parameters of Table 2. $[Ba] = 3.3 \cdot 10^{-10}$ M.

The complexation reactions of alkalis with silanol groups (weak and strong) are expressed by:

$$SiOH + M^+ \underset{K_{C,M}}{\Leftrightarrow} SiOM + H^+ \quad (5c)$$

and for ionic exchange:

$$X_2Ca + 2M^+ \leftrightarrow 2XM + Ca^{2+} \quad (9)$$

The proposed logK obtained by fit for the respective reactions, for M^+ adsorption in C-S-H (0.8), are reported in Table 2.

Including these reactions to the sorption model, the experimental data of Ba sorption in the presence of M^+, could be simulated (continuous line in Fig. 7). In the absence of additional and more detailed sorption data of the alkali on all the C-S-H phases, it is impossible to assert that these parameters are exact or unique but, at this stage, they can be used operationally to analyze more in depth Ba adsorption processes on C-S-H phases or in HCP under more complex chemical conditions.

4. Conclusions

The adsorption of Ba on C-S-H phases has been experimentally analysed using four gels at different Ca/Si ratio (from 0.8 to 1.6). Sorption of Ba clearly depends on the Ca/Si ratio and decreases when the ratio increases.

A sorption model accounting for both Ba retention behaviour and the changes observed in surface charge upon its adsorption at high concentrations has been developed. The model includes surface complexation of Ba on two silanol-like sites (weak and strong sites) and ion exchange with Ca on a third site. The trend and magnitude of the surface potential derived by sorption, agrees satisfactorily with experimental ζ-potentials in all the cases. This could not be attained considering 1 site (either cationic exchange or surface complexation) model.

The model reproduces very well the adsorption of Ba in the three phases with the lower Ca/Si, and slightly over-predicts adsorption in C-S-H (1.6). The phase with the highest Ca/Si ratio shows the lowest N_2-BET and shows 65% less sorption capacity. This can be explained supposing that structural modifications occur in the C-S-H gels, as Ca content increases, which reduce the number of accessible sorption sites (for example for increase of the mean particle grain size or for particle compaction), but also assuming that portlandite has been formed

during the preparation of the C-S-H phases. Portlandite, in fact, does not sorb Ba significantly.

Sorption of Ba on C-S-H is affected by the presence of alkalis at relatively high concentrations. The decrease of the distribution coefficient for Ba on at trace concentration is quantifiable when the alkalis concentration is above $1 \cdot 10^{-3}$ M. The most competitive ion to Ba adsorption is potassium and the less competitive is sodium. This competition could be accounted for including the respective sorption reactions for the alkalis in the C-S-H gels with the proposed three sites model.

Acknowledgements

This work has been carried out under the frame of the MIRAME Project (CTM2014-60482-P) supported by the Spanish Ministry of Economy and Competiveness. μPIXE analyses were funded by the European Union's HORIZON 2020 Program under grant agreement 654002 (ENSAR2). The comments and remarks of two anonymous reviewers are greatly acknowledged.

References

[1] M. Atkins, F.P. Glasser, Application of Portland cement-based materials to radioactive waste immobilization, Waste Manag. 12 (1992) 105–131.
[2] F.P. Glasser, Chemistry of cement-solidified waste forms, in: R.D. Spence (Ed.), Chemistry and Microstructure of Solidified Waste Forms, Lewis Publishers, New York, 1993.
[3] Q.Y. Chen, M. Tyrer, C.D. Hills, X.M. Yang, P. Carey, Immobilisation of heavy metal in cement-based solidification/stabilisation: a review, Waste Manag. (1993) 29 (1) (2000) 390–403.
[4] N.D.M. Evans, Binding mechanisms of radionuclide to cement, Cem. Concr. Res. 38 (2007) 543–553.
[5] M. Ochs, D. Mallants, L. Wang, Radionuclide and metal sorption on cement and concrete, Topics in Safety, Risk, Reliability and Quality, Springer, Switzerland, 2015.
[6] B. Batchelor, Overview of waste stabilisation with cement, Waste Manag. 26 (2006) 689–698.
[7] J. Tits, K. Iijima, E. Wieland, G. Kamei, The uptake of radium by calcium silicate hydrates and hardened cement paste, Radiochim. Acta 94 (2006) 637–643.
[8] S. Aggarwal, M.J. Angus, J. Ketchen, Sorption of radionuclides onto specific mineral phases present in repository cements, NSS/R312, AEA-DandR-0395 Technical Report, 2000.
[9] I. Pointeau, Etude mécanistique et modélisation de la retention de radionucléides par les phases de silicate de calcium des ciments hydrates, Thèse de l'Université de Reims-Champagne Ardennes, France, 2000.
[10] H.F.W. Taylor, Cement Chemistry, Thomas Telford, 1997 459.
[11] J.J. Chen, J.J. Thomas, H.F.W. Taylor, H.M. Jennings, Solubility and structure of calcium silicate hydrate, Cem. Concr. Res. 74 (2004) 1499–1519.
[12] J.E. Rossen, B. Lothenbach, K.L. Scrivener, Composition of C-S-H in pastes with increasing level of silica, Cem. Concr. Res. 75 (2015) 14–22.
[13] G. Renaudin, J. Russias, F. Leroux, F. Frizon, C. Cau-dit-Coumes, Structural characterisation of C-S-H and C-A-S-H samples-part I: long range order investigated by Rietveld analyses, J. Solid State Chem. 182 (2009) 3312–3319.
[14] I.G. Richardson, The calcium silicate hydrates, Cem. Concr. Res. 38 (2008) 137–158.
[15] B. Lothenbach, A. Nonat, Calcium silicate hidrates: solid and liquid phase composition, Cem. Concr. Res. 78 (2015) 57–70.
[16] F.T. Ewart, S. Terry, S.J. Williams, Near-field sorption data for caesium and strontium, AERE-M 3452 Technical Report, 1985.
[17] T.R. Holland, D.J. Lee, Radionuclide getters in cement, Cem. Concr. Res. 22 (1992) 247–258.
[18] S. Bayliss, R.M. Howse, R. McCrohon, P. Oliver, Near-field sorption studies, AEAT/ERRA-0073 Technical Report, 2000.
[19] J. Tits, E. Wieland, J.P. Dobler, D. Kunz, The uptake of strontium by calcium silicate hydrates under high pH conditions: an experimental approach to distinguish adsorption from co-precipitation processes, Proceedings of the Material Research Society Symposium, 807, 2004, pp. 689–694.
[20] J. Tits, E. Wieland, C.J. Muller, C. Landesmann, M.H. Bradbury, A wet chemistry study of the strontium binding by calcium silicate hydrates, J. Colloid Interface Sci. 300 (2006) 78–87.
[21] E. Wieland, J. Tits, D. Kunz, R. Dahn, Strontium uptake by cementitious, Environ. Sci. Technol. 42 (2008) 403–409.
[22] T. Iwaida, S. Nagasaki, S. Tanaka, Sorption study of strontium onto hydrated cement phases using a sequential desorption method, Radiochim. Acta 88 (2000) 483–486.
[23] H. Viallis-Terrise, A. Nonat, J.C. Petit, J. Colloid Interface Sci. 244 (1) (2001) 58–65.
[24] H. Viallis-Terrise, P. Faucon, J.C. Petit, A. Nonat, Interactions between salts (NaCl and CsCl) and C-S-H, J. Phys. Chem. B 103 (25) (1999) 5212–5219.
[25] P.C. Zhang, P.V. Brady, S.E. Arthur, W.Q. Zhou, D. Sawyer, D.A. Hesterberg, Adsorption of Ba(II) on montmorillonite: an EXAFS study, Colloids Surf. A 190 (2001) 239–249.
[26] S.Y. Hong, F.P. Glasser, Alkali binding in cement pastes. Part I. The CSH phases, Cem. Concr. Res. 29 (1999) 1893–1903.
[27] I. Horcas, R. Fernández, M. Gómez-Rodriguez, J. Colchero, J. Gómez-Herrero, A.M. Baro, WSXM: a software for scanning probe microscopy and a tool for nanotechnology, Rev. Sci. Instrum. 78 (2007) 013705.
[28] R.J. Hunter, Zeta Potential in Colloid Science, Academic Press, 1981 398.
[29] I. Pointeau, P. Reiller, N. Macé, C. Landesman, N. Coreau, Measurement and modelling of the surface potential evolution of hydrated cement pastes as a function of degradation, J. Colloid Interface Sci. 300 (2006) 33–44.
[30] C. Labbez, I. Pochard, B. Jonsson, A. Nonat, CSH/solution interface: experimental and Monte Carlo studies, Cem. Concr. Res. 41 (2011) 161–168.
[31] A. Nonat, The structure and stoichiometry of C-S-H, Cem. Concr. Res. 24 (2004) 1521–1528.
[32] C.P. Huang, W. Stumm, Specific adsorption of cations hydrous Al_2O_3, J. Colloid Interface Sci. 231-259 (1973).
[33] D.A. Dzombak, F.M. Morel, Surface Complexation Modelling: Hydrous Ferric Oxide, John Wiley and Sons, 1990.
[34] J. Van der Lee, L. de Windt, CHESS tutorial and cookbook, Technical Report LHM/RD/99/05, 1999.
[35] Van der Lee, "Modelisation du comportement geoquímique et du transport des radionucleides en presence de colloides" Thesis, Écóle National Superieure des Mines de Paris, 1997.
[36] T.G. Heat, D.J. Illet, J. Tweed, Thermodynamic modelling of the sorption of radioelement onto cementitious materials, Mater. Res. Soc. Symp. Proc. 412 (1996) 443–449.
[37] S.V. Churakov, C. Labbez, L. Pegado, M. Sulpizi, Intrinsic acidity of surface sites in calcium silicate hydrates and its implications to their electrokinetics properties, J. Phys. Chem. C 118 (2014) 11752–11762.
[38] E. Papirer, Adsorption on Silica Surfaces, Marcel Dekker, NY, 2000 (ISBN-13: 978-0824700034).
[39] E. Osthols, Thorium sorption on amorphous silica, Geochim. Cosmochim. Acta 59 (7) (1995) 1235–1249.
[40] O.P. Shrivastava, F.P. Glasser, Ion exchange properties of $Ca_5Si_6O_{18}H_2$ $4H_2O$, J. Mater. Sci. Lett. 4 (1985) 1122–1124.
[41] O.P. Shrivastava, F.P. Glasser, Ion exchange properties 11 Å tobermorite, Reactivity of Solids, 2, 1986, pp. 261–268.
[42] D.E. Yates, T.W. Healy, The structure of the silica/electrolyte interface, J. Colloid Interface Sci. 55 (1) (1975) 9–19.
[43] R.O. James, G.A. Parks, Characterisation of aqueous chemical colloids by electrical double layer and intrinsic surface chemical properties, Surf. Colloid Sci. 12 (1982) 119–216.
[44] L. Nachbaur, P.C. Nkinamubanzi, A. Nonat, J.C. Moutin, Electrokinetic properties which controls the coagulation of silicate cement suspensions during early stage hydration, J. Colloid Interface Sci. 202 (1998) 261.
[45] C. Labbez, A. Nonat, I. Pochard, Jonsson, Experimental and theoretical evidence of overcharging of calcium silicate hydrate, J. Colloid Interface Sci. 309 (2007) 303–307.
[46] T. Iwaida, S. Nagasaki, S. Tanaka, T. Yaita, S. Tachimori, Structure alteration of C-S-H caused by sorption of caesium, Radiochim. Acta 90 (2002) 677–681.